



## Gd/HZSM-5 catalyst for conversion of methanol to hydrocarbons: Effects of amounts of the Gd loading and catalyst preparation method



Sungtak Kim<sup>a,\*</sup>, Gyungah Park<sup>a</sup>, Seok Ki Kim<sup>a,b</sup>, Yong Tae Kim<sup>a,b</sup>, Ki-Won Jun<sup>a,b</sup>, Geunjae Kwak<sup>a,b,\*</sup>

<sup>a</sup> Carbon Resources Conversion Catalytic Research Center, Korea Research Institute of Chemical Technology (KRICT), P.O. Box 107, Gajeongro 141, Yuseong, Daejeon 34114, Republic of Korea

<sup>b</sup> Advanced Materials and Chemical Engineering, University of Science & Technology, Daejeon 34113, Republic of Korea

### ARTICLE INFO

**Keywords:**

Gadolinium  
Coke  
ZSM-5  
Deactivation  
Methanol-to-hydrocarbons

### ABSTRACT

In this work, the effect of the gadolinium (Gd) content and preparation method on the characteristics of Gd-modified HZSM-5 catalysts and their reactivity in a methanol-to-hydrocarbons (MTH) reaction has been studied in detail. Gd/HZSM-5 catalysts with Gd contents of 1 wt% (1GdHZ), 5 wt% (5GdHZ), and 10 wt% (10GdHZ) were prepared by an incipient wet impregnation method, and another Gd-modified HZSM-5 catalyst (GdHZ<sub>IE</sub>) was prepared by an ion exchange method. It was found that increasing the Gd content in the catalysts prepared via the impregnation method with uniformly distributed nano-sized particles and thin films of Gd<sub>2</sub>O<sub>3</sub> directly influenced the crystallinity, surface area, pore volume, acid-base properties, and reactivity of the catalysts. In particular, the amount of Lewis acid sites (LAS) on the catalyst determine the selectivity of light olefins and aromatics during the MTH reaction. In contrast, the GdHZ<sub>IE</sub> catalyst possess a larger number of strong LAS and show higher aromatic selectivities compared with the bare HZSM-5 catalyst. Regardless of the preparation method, the catalyst modification by Gd inhibited the formation of polycondensed aromatic species on the catalyst surface and reduced the amount of carbon deposition by more than 50%. As the increasing amounts of Gd reduced the amount of carbon deposition, the lifetimes of the Gd/HZSM-5 catalysts were also prolonged.

### 1. Introduction

Owing to the presence of high-density acid sites on their surfaces and the property of shape selectivity, zeolite-based solid acid catalysts have been used for naphtha cracking since the 1950s. They are now widely used as cracking catalysts throughout the petrochemical industry [1–3]. Zeolite-based catalysts have also been employed in a variety of processes related to carbon-resource conversion because of their inherent chemical and physical properties [3–7]. Recently, the process of converting methanol into value-added hydrocarbons (methanol-to-hydrocarbons, MTH) such as light olefins or aromatics over solid acid catalysts has been studied extensively in an effort to develop a sustainable energy source [4,5]. Methanol can be mass-produced from synthesis gas (CO + H<sub>2</sub>), which is produced by coal gasification or reforming methane and biomass. The Fischer-Tropsch (FT) process enables direct conversion of synthesis gas to hydrocarbons and even though the MTH process requires one more step than the FT process, the high selectivity for the target product emanating from the use of

zeolite catalysts offsets the shortcomings of the MTH process [4,8].

The ZSM-5 zeolite is a highly active catalyst and is used to produce hydrocarbons, especially aromatic compounds, from methanol because of its strong acid sites and unique pore structure [5,9,10]. However, carbocation intermediates formed during the MTH reactions are readily adsorb on the strong acidic sites of zeolite catalysts and form polycondensed aromatics consisting of several benzene rings via a sequence of growth mechanisms. This eventually results in the blocking of active sites, pore mouths, and intersections in the zeolite catalyst (so-called “coking”) [7,11–14]. Thus, despite the high activity and selectivity of the zeolite catalysts, this severe deactivation from coking is a major problem for their application in commercial MTH plants.

The acid sites are typically located on the surface and in the pores of the zeolite, and they are also the active sites for the MTH reaction and responsible for the excellent reactivity of the catalyst. The hydrocarbon intermediates or cations produced during the reaction are readily and strongly adsorbed onto these sites [15,16]. The once-adsorbed hydrocarbon intermediates on the surface and/or in the pores of the zeolite

\* Corresponding authors at: Carbon Resources Conversion Catalytic Research Center, Korea Research Institute of Chemical Technology (KRICT), P.O. Box 107, Gajeongro 141, Yuseong, Daejeon 34114, Republic of Korea

E-mail addresses: [kimst@kRICT.re.kr](mailto:kimst@kRICT.re.kr) (S. Kim), [gkwak@kRICT.re.kr](mailto:gkwak@kRICT.re.kr) (G. Kwak).

catalysts grow as aromatic carbon compounds via oligomerization, hydrogenation and dehydrogenation, cyclization, and aromatization; on a surface without any restrictions on their growth, poly-condensed aromatics can cover the active sites or pore openings, and even block the zeolite pores from inside to disturb the diffusion of reactants into the active sites [12,13,15,17]. As a result, the diffusion and contact of the reactant with the active sites on the surface and those located in the pores are intrinsically blocked, and the zeolite catalyst rapidly becomes inactive.

Various methods have been used to try to diminish the rapid deactivation of the ZSM-5 zeolite catalysts by carbon deposition. One of these methods involves the synthesis of nano-sized or hierarchically structured zeolite crystals by an alkali treatment or bottom-up synthesis in order to improve the diffusivity of the reactants to the active sites [18–21]. In this case of morphological modification, the deactivation of ZSM-5 zeolite catalysts by pore clogging is reduced and the lifetime of the catalyst is thereby increased. However, the increase in the diffusion and surface area by zeolite structure control does not reduce the rate and amount of carbon deposition [17]. Another strategy to improve catalyst deactivation by coke formation is to reduce the amount of acid sites, especially Brønsted or Lewis acid sites, by either increasing the Si/Al ratio during zeolite synthesis or via ion exchange with metal cations to prevent the adsorption of the hydrocarbon intermediates formed during the reaction [17,22,23]. Although this method has a clear effect in terms of prolonging the catalyst lifetime, the catalytic activity of the zeolite simultaneously decreases owing to the reduced number of acid sites. Therefore, this method is not useful for reactions that require a catalyst with highly acidic active sites.

Yet another method to prevent catalyst deactivation by coke formation during the MTH reaction is to modify the ZSM-5 zeolite catalyst with a small amount of metal acting as a coke inhibitor. Noble metals such as platinum and gold have been shown to catalyze the hydrogenation of ZSM-5 catalysts by interfering in the formation of condensed aromatics or graphite coke [24–26]. The use of rare earth metals for the same purpose has also attracted interest because of their relatively low cost and abundance. A Gd-promoted ZSM-5 catalyst has recently been shown to have excellent anti-coking abilities for chemical conversion of hydrocarbons. Kim and co-workers have recently found that the adsorption of carbocations and formation of complex aromatics structured coke is impeded during hydrocarbon cracking and methanol conversion reactions on the modified ZSM-5 catalyst surface on which  $\text{Gd}_2\text{O}_3$  is present uniformly in the form of nano-sized particles or thin films, which improves the lifetime of the catalyst [27–29]. Nevertheless, the use of Gd metal as a coke inhibitor still needs to be studied for a deeper understanding into its mechanism. Hence, in this work, the changes in the physicochemical properties of the Gd/HZSM-5 catalysts and the catalytic activities in a MTH reaction were studied according to the different Gd loading amounts and the preparation method.

## 2. Experimental

### 2.1. Catalyst preparation

The Gd/HZSM-5 catalysts were firstly prepared by an incipient wet impregnation method.  $\text{NH}_4\text{-ZSM-5}$  (Zeolyst CBV 5524G, Si/Al = 25) was calcined in a muffle furnace under the flow of air at 600 °C for 6 h to prepare HZSM-5. Gd precursor ( $\text{Gd}(\text{NO}_3)_3 \cdot 6\text{H}_2\text{O}$ , Sigma-Aldrich) satisfying ca. 1 wt%, 5 wt%, and 10 wt% of the Gd content was dissolved in de-ionized water, which amount is slightly above the pore volume of the HZSM-5, and the solution and HZSM-5 were mixed and stirred well. The Gd/HZSM-5 catalysts, denoted as 1GdHZ, 5GdHZ, and 10GdHZ, were finally obtained after dry at 110 °C for overnight and calcination at 550 °C for 5 h.

The Gd/HZSM-5 catalyst was also prepared by ion exchange method. The prepared HZSM-5 was added into 0.15 M of aqueous solutions of Gd precursor with a ratio of 50 (ml<sub>solution</sub>) to 1 (g<sub>HZSM-5</sub>). Ion

exchange was accomplished under stirring at 80 °C for 12 h, and the slurry was washed by de-ionized water, dried at 110 °C overnight. After three subsequent ion exchange processes, a final calcination step was performed in air for 5 h at 550 °C to remove any residual precursor salt materials and oxidize the active metals. The obtained samples was denoted as GdHZ<sub>IE</sub>, the bare HZSM-5 was denoted as HZ for comparison.

### 2.2. Catalyst characterization

Powder X-ray diffraction (XRD) was assigned to identify peak shape and relative crystallinity for the prepared Gd/HZSM-5 catalysts. A Rigaku D/MAX IIIB X-ray diffractometer equipped with Cu-K $\alpha$  radiations was used for bulk phase analysis. All spectra were collected at 20 values between 3° and 80° using a step size of 0.02° and 2 s per step.

Inductively coupled plasma-atomic emission spectroscopy (ICP-AES) was carried out to measure the Gd loading using an iCAP 6500 (Thermo Scientific)

$\text{N}_2$  adsorption-desorption analysis was carried out using TriStar 3000 (Micromeritics) at a temperature of –196 °C. Before the adsorption-desorption measurements, all of the Gd/HZSM-5 catalysts were degassed at 300 °C under  $1.0 \times 10^{-6}$  Torr for 4 h.

Scanning electron microscopy (SEM) images of the Gd/HZSM-5 catalysts were obtained using a Zeiss UltraPlus Thermal Field Emission Scanning Electron Microscope.

Scanning transmission electron microscopy (STEM) imaging and energy dispersive X-ray spectroscopy (EDS) analysis were conducted using a TalosTM F200S transmission electron microscope (FEI), which at 200 kV provides a nominal probe size of < 0.12 nm.

Temperature programmed desorption of ammonia and carbon dioxide ( $\text{NH}_3\text{-TPD}$  &  $\text{CO}_2\text{-TPD}$ ) were performed on an Autochem II 2920 of Micromeritics instrument. Before the TPD analysis, all the catalysts were pretreated at 600 °C with flowing He gas for 1 h in order to remove any adsorbed water and saturated with  $\text{NH}_3$  gas (15%, balanced with He, flow rate: 50 mL/min) or  $\text{CO}_2$  gas (10%, balanced with He, flow rate: 50 mL/min) for 30 min at a temperature of 100 °C. After the saturation stage, the catalysts were purged with flowing He gas for 1 h to remove weakly adsorbed  $\text{NH}_3$  or  $\text{CO}_2$  molecules on the surface. Finally, TPD measurement was carried out with maintaining a ramping rate of 10 °C/min from 100 °C to 600 °C with flowing pure He gas.

Brønsted (BAS) and Lewis acid sites (LAS) were determined via pyridine adsorption-desorption experiments in a stainless steel variable temperature gas flow transmission cell using a Fourier transform infrared (FT-IR) spectrometer equipped with a mercury-cadmium-telluride-B detector (Nicolet Nexus 4700). 30 mg of the powder catalyst samples were prepared as self-supporting pellets with a diameter of 12 mm and placed in the cell. After pre-treatment at 250 °C to remove adsorbed water, pyridine vapor was introduced into the cell from a saturator with flowing pure He gas at 150 °C for 20 min. Then, pure He gas was purged through the catalyst pellet at 150 °C for 3 h to remove any physically adsorbed pyridine molecules prior to the collection of the IR spectra. The IR spectra of adsorbed pyridine molecules on the surface of the catalyst were recorded from 1400  $\text{cm}^{-1}$  to 1700  $\text{cm}^{-1}$ , and both chemisorbed pyridinium ion ( $\text{PyH}^+$ ) on Brønsted acid sites and pyridine bonded on Lewis acid sites ( $\text{PyL}$ ) were quantified at 1545  $\text{cm}^{-1}$  and 1455  $\text{cm}^{-1}$ , respectively. The extinction coefficients were taken to be 1.13  $\text{cm} \cdot \text{mmol}^{-1}$  ( $\text{PyH}^+$ ) and 1.28  $\text{cm} \cdot \mu\text{mol}^{-1}$  ( $\text{PyL}$ ), respectively for estimation of acid sites [30]. The quantity of BAS and LAS were calculated from the formula presented below (Beer-Lambert's law):

$$C = \frac{A}{\varepsilon} \times \frac{S}{m} \times 1000$$

where C is the concentration of acid sites ( $\mu\text{mol g}^{-1}$ ), A is the area of band ( $\text{cm}^{-1}$ ), S is the surface of the wafer ( $\text{cm}^2$ ),  $\varepsilon$  is the molar extinction coefficient ( $\text{cm} \cdot \mu\text{mol}^{-1}$ ), and m is the mass of sample (mg).

Temperature programmed oxidation (TPO) experiment was carried out using an Autochem II 2920 of Micromeritics instrument to determine burn-off properties of carbon deposits of the catalyst collected after 20 h MTH reaction at 400 °C. Prior to TPO, the samples were pretreated at 200 °C with flowing pure He gas to eliminate the adsorbed water and volatile compounds on the surface. Finally, TPO measurement was carried out with maintaining a ramping rate of 10 °C/min from 100 °C to 600 °C with flowing O<sub>2</sub> gas (10%, balanced with He, flow rate: 100 mL/min).

IR spectra of the spent catalysts were collected using the same FTIR spectrometer described above. The spectra of the samples were collected in single beam absorbance mode with a spectral resolution of 4 cm<sup>-1</sup> at room temperature.

### 2.3. Catalyst evaluation: methanol-to-hydrocarbons reaction

Methanol to hydrocarbons reaction was conducted in 1/2" stainless steel reactor of fixed-bed type reactor system. 1 g of each catalyst, which was sieved to 20–40 mesh size (or particle size around 0.85 mm) and diluted with 3 g of SiC, was placed in the center of the reactor. Prior to each reaction, the catalyst was pretreated in N<sub>2</sub> with a rate of 100 mL/min at 400 °C for 3 h to remove contaminants on the sample. After pretreatment, the temperature was maintained, and pure methanol feed was provided with a flow rate of 0.1 mL/min by Younglin YL 9200 pump, satisfying weight hourly space velocity (WHSV) of 4.75 g<sub>methanol</sub> g<sub>catalyst</sub><sup>-1</sup> h<sup>-1</sup>. The effluent products were analyzed by Younglin 6100GC equipped with Rtx-DHA (0.25 mm ID x 100 m, Restek) linked FID. Methanol to hydrocarbons reactions over the bare HZSM-5 and the Gd/HZSM-5 catalysts were performed at 1 bar, 400 °C for 70 h. Methanol conversion and product selectivity were calculated by the equation below.

$$\text{Methanol conversion}(\%) = \frac{\text{Methanol in} - \text{Methanol out}}{\text{Methanol in}} \times 100$$

$$\text{Products selectivity}(C-\%) = \frac{C_i, \text{ out as a product}}{C_{\text{total, out as a product}}} \times 100$$

## 3. Results and discussion

### 3.1. Catalyst characterization

The X-ray diffraction (XRD) patterns of the prepared Gd/HZSM-5 catalysts shown in Fig. 1 confirm that all of them have the typical MFI structure. Shape changes or pattern shifts were not observed, indicating that the content of Gd on HZSM-5 does not change the crystalline structure of pure ZSM-5; however, the intensity of the XRD pattern decreases with increasing amounts of Gd. The intensity of the XRD

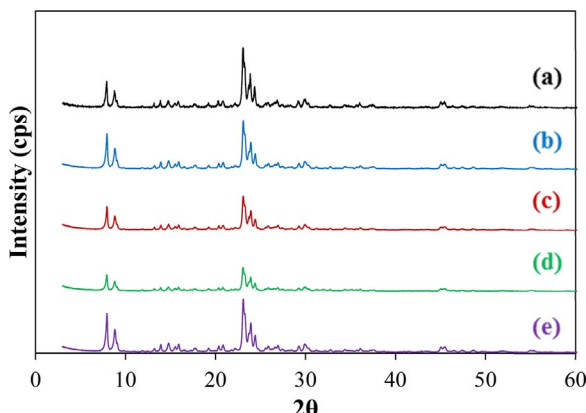


Fig. 1. XRD patterns of the (a) HZ, (b) 1GdHZ, (c) 5GdHZ, (d) 10GdHZ, and (e) GdHZ<sub>IE</sub> catalysts.

**Table 1**  
Gd loading and textural properties of the bare and Gd modified HZSM-5 catalysts.

	Gd (wt %) <sup>a</sup>	S <sub>BET</sub> (m <sup>2</sup> / g) <sup>b</sup>	S <sub>Ext</sub> (m <sup>2</sup> / g) <sup>b</sup>	Pore Size (Å) <sup>b</sup>	V <sub>Total</sub> (cm <sup>3</sup> /g) <sup>b</sup>	V <sub>Micro</sub> (cm <sup>3</sup> /g) <sup>b</sup>	V <sub>Meso</sub> (cm <sup>3</sup> /g) <sup>b</sup>
HZ	N/A	405	67.8	24.9	0.252	0.138	0.111
1GdHZ	1.03	389	55.5	24.9	0.239	0.131	0.103
5GdHZ	4.82	359	52.6	24.2	0.224	0.122	0.097
10GdHZ	9.76	331	50.8	23.9	0.198	0.107	0.086
GdHZ <sub>IE</sub>	3.54	390	71.1	31.4	0.278	0.139	0.128

<sup>a</sup> Gd content was determined by inductively coupled plasma (ICP) analysis.

<sup>b</sup> S<sub>BET</sub> refers to the BET surface area; S<sub>Ext</sub> refers to the external surface area calculated using the t-plot method; V<sub>Total</sub> refers to the total pore volume based on single point adsorption; V<sub>Micro</sub> refers to the micropore volume measured using the t-plot method; V<sub>Meso</sub> refers to the mesopore volume based on Barrett-Joyner-Halenda adsorption.

pattern of the catalyst prepared by the ion exchange method (GdHZ<sub>IE</sub>) was not reduced. Instead, its observed intensity was similar to that of the bare ZSM-5 (HZ), even though its Gd content is similar to that of the 5GdHZ catalyst (Table 1). The XRD patterns did not show the formation of Gd metal particles or Gd oxides in any of the Gd-loaded catalysts.

Table 1 summarizes the Gd content and textural properties of the bare ZSM-5 and the Gd/HZSM-5 catalysts. The experimentally determined Gd contents for the catalysts prepared by the impregnation method were similar to the calculated target values. The Brunauer-Emmett-Teller (BET) surface area, external surface area, and pore volume (including the micro- and mesopore volumes) showed maximum values for HZ. These attributes decreased linearly as the Gd content on HZSM-5 was increased. On the other hand, the mesopore volume and total pore volume of the GdHZ<sub>IE</sub> catalyst increased by ca. 10% in comparison with that for the HZ catalyst.

The FE-SEM and STEM images of the prepared catalysts were compared to determine the location of Gd metal on the HZSM-5 crystals. Although this information could not be confirmed from the FE-SEM image (Fig. S1), the signal of Gd in the EDS mappings revealed that Gd is uniformly distributed on the surface of the crystals (Fig. S2). However, the bright field STEM images of the 10GdHZ catalyst (Fig. 2A,C) showed that a crystalline thin film of thickness 2–5 nm had covered the surface of the HZSM-5 crystal. In addition, the EDS elemental mapping identified uniformly distributed Gd atoms on the crystal (Fig. 2D). When the catalysts are prepared by the impregnation method, Gd metal is mostly present as a thin film on the catalyst surface with a very small amount existing in the shape of a horn or a hook (Fig. 2B). Although it is not shown in this paper, increasing the Gd loading on HZSM-5 does not affect the film thickness; it only affects the amount of film-covered crystals.

One of the other major features besides the shape selectivity of the zeolite material as a catalyst is that these catalysts exhibit strong acidity. The catalytic activity and selectivity of the product formed in the reaction are determined by the inherent acidity of these solid acid catalysts, which can be modified by addition of various metal atoms [31]. Thus, the acid characteristics of the prepared Gd/HZSM-5 catalysts were investigated via NH<sub>3</sub>-TPD and using a pyridine adsorption-desorption in situ transmittance cell. The NH<sub>3</sub>-TPD curves of the catalysts given in Fig. 3 showed that desorption of ammonia occurred strongly in two temperature zones; while desorption at temperatures from 100 °C to 250 °C was attributed to weakly acidic sites, desorption taking place from 250 °C to 600 °C was associated with strongly acidic sites. In the case of the HZ catalyst, the area of weak and strong acid sites could be clearly distinguished, and the results of quantitative analysis by peak deconvolution given in Table 2 show that the quantity of strong acid sites is 42.5% more than that of the weak acid sites. Py-IR spectra are shown in Fig. S3. As the Gd content was increased, the peaks in the low and high temperature zones became wider and lower, respectively. Furthermore, the amount of the weak acid sites also increased accordingly and the amount of strong acid sites decreased with

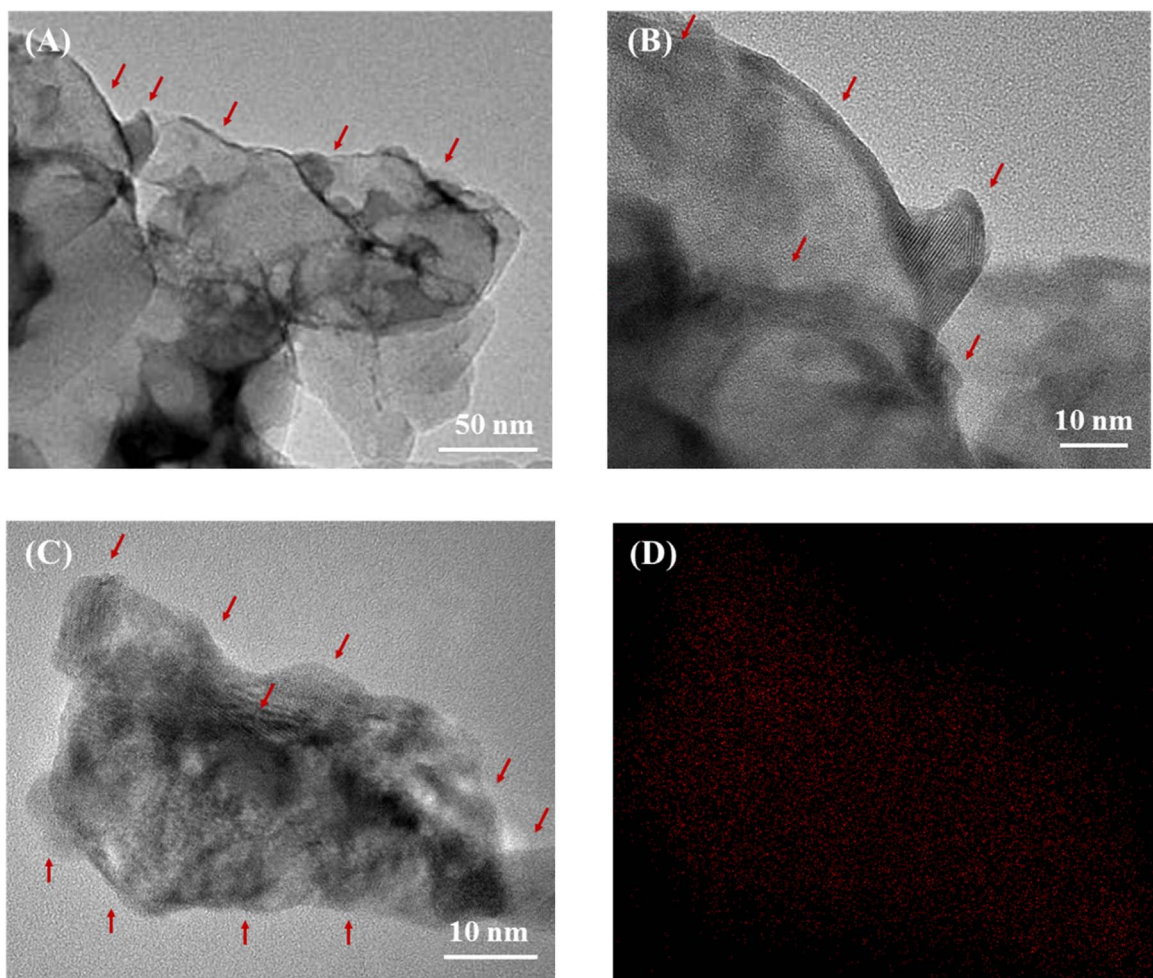


**Fig. 2.** STEM images (bright field) of the 10GdHZ catalyst (A–C), EDS mapping of Gd (corresponding to the image in C) (D). The red arrows indicate crystalline lattice and the thin film formed by Gd on the 10GdHZ catalyst. (For interpretation of the references to colour in this figure legend, the reader is referred to the web version of this article.)

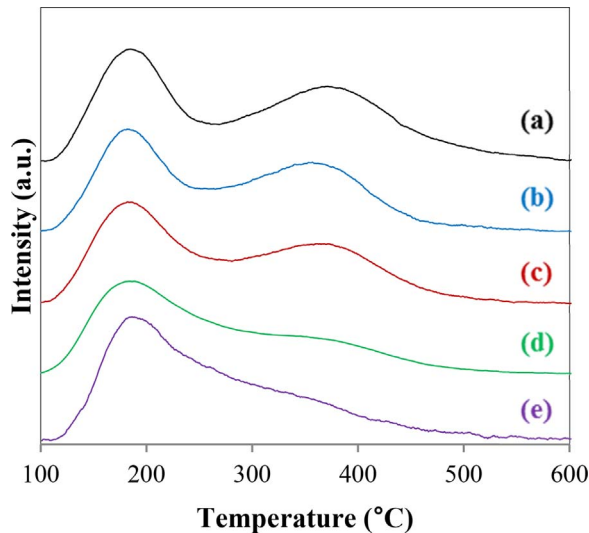


**Fig. 3.** NH<sub>3</sub>-TPD curves of the (a) HZ, (b) 1GdHZ, (c) 5GdHZ, (d) 10GdHZ, and (e) GdHZ<sub>IE</sub> catalysts.

increasing Gd content (Table 2). Unlike the 5GdHZ catalyst, most of the acid sites of the GdHZ<sub>IE</sub> catalyst were weakly acidic, and the amount of strong acid sites was similar to the amount of the 10GdHZ catalyst. Despite a possibility of misinterpretation of the TPD spectra owing to adsorption of the desorbed ammonia molecules during the analysis

[32], the Py-IR analysis shows a similar trend as elucidated from the NH<sub>3</sub>-TPD results (Table 2). It is worth noting that the amount of strong Lewis acid sites and L/B<sub>strong</sub> increased significantly in the GdHZ<sub>IE</sub> catalyst in comparison to those in the HZ catalyst (about twice and seven times).

The base properties of the bare and Gd-modified HZSM-5 catalysts were determined by CO<sub>2</sub>-TPD. The results of these experiments are shown in Fig. 4. As the Gd content was increased, the maximum intensity of the CO<sub>2</sub> desorption peak shifted toward higher temperatures. In addition, the quantity of basic sites also increased with increasing Gd content (Table S1), indicating that the basic characteristic of the catalyst was improved. For the catalyst synthesized by the ion exchange method (GdHZ<sub>IE</sub>), the temperature of the maximum desorption peak and its quantity of basic sites were similar to those determined for the 5GdHZ catalyst. Therefore, it may be concluded that the base characteristics of the Gd-modified HZSM-5 catalyst are only related to the Gd content and do not depend on the preparation method.

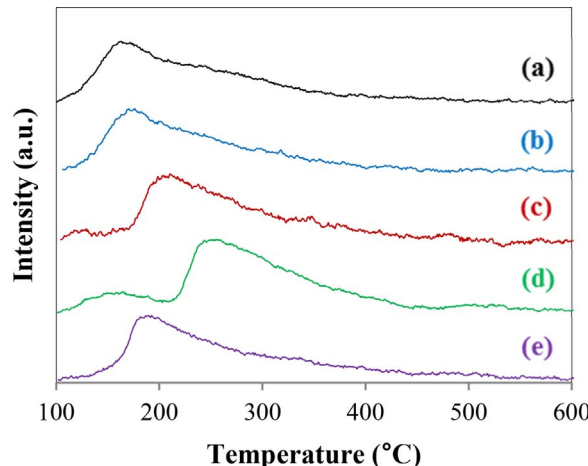
### 3.2. Catalytic performance test

The catalytic activities of the Gd/HZSM-5 catalysts were evaluated during a MTH reaction. The temperature of 400 °C was selected because the MTH reaction is dominant at this temperature [10]. The methanol conversions and product selectivities at 6 h after reaction initiation for each catalyst are summarized in Table 3. It should be noted that because the product selectivity was recorded at the very initial reaction time, the amount of coke could be negligible. For all cases, the

**Table 2**

Summary of acid quantity of the Gd/HZSM-5 catalysts.

	Acid sites <sup>a</sup> (mmol g <sup>-1</sup> )			Weak acid sites <sup>b</sup> (mmol g <sup>-1</sup> )			Strong acid sites <sup>b</sup> (mmol g <sup>-1</sup> )			L/B <sup>c</sup>	
	Weak	Strong	Total	Lewis	Brønsted	Total	Lewis	Brønsted	Total	Strong	Total
HZ	0.273	0.389	0.662	0.005	0.087	0.092	0.057	0.236	0.293	0.24	0.19
1GdHZ	0.275	0.359	0.634	0.006	0.083	0.089	0.032	0.174	0.206	0.18	0.15
5GdHZ	0.326	0.320	0.645	0.007	0.103	0.110	0.019	0.123	0.142	0.15	0.12
10GdHZ	0.387	0.198	0.585	0.006	0.104	0.110	0.003	0.100	0.103	0.03	0.04
GdHZ-IE	0.423	0.203	0.626	0.040	0.122	0.162	0.108	0.061	0.169	1.77	0.81

<sup>a</sup> The acid quantity of the catalysts were calculated by deconvolution of the NH<sub>3</sub>-TPD curves with Gaussian peaks ( $R^2 > 0.99$ ).<sup>b</sup> The quantity of the weak and strong acid sites were determined by Py-IR; the strong acid sites were obtained from Py-IR spectra at 350 °C, and the weak acid sites were calculated by subtracting the acid quantity at 350 °C from the acid quantity at 150 °C.<sup>c</sup> L/B means the ratio of the quantity of Lewis acid to the quantity of Brønsted acid.**Fig. 4.** CO<sub>2</sub>-TPD curves of the (a) HZ, (b) 1GdHZ, (c) 5GdHZ, (d) 10GdHZ, and (e) GdHZ-IE catalysts.**Table 3**

Product selectivity from the Gd-modified HZSM-5 catalysts after 6 h on stream during the MTH reaction.

	HZ	1GdHZ	5GdHZ	10GdHZ	GdHZ-IE
MeOH conversion (%)	100	100	100	100	100
Dimethyl ether	0.0	0.0	0.0	0.0	0
CH <sub>4</sub>	2.3	1.9	1.0	1.4	1.5
C <sub>2</sub> H <sub>4</sub>	3.6	5.7	4.6	0.2	5.2
C <sub>3</sub> H <sub>6</sub>	3.6	8.6	7.1	19.5	6.4
C <sub>4</sub> H <sub>8</sub>	4.4	7.4	7.6	15.0	5.4
C <sub>2</sub> =C <sub>4</sub> = <sup>a</sup>	11.6	21.7	19.2	34.8	17.0
C <sub>5</sub> =C <sub>6</sub> =	14.5	16.4	19.7	21.8	15.4
Paraffins (C <sub>2</sub> –C <sub>5</sub> )	33.2	28.1	25.7	19.5	16.7
Benzene	1.9	1.7	0.9	0.5	0.7
Toluene	9.0	7.5	5.8	4.0	3.6
Ethylbenzene	1.0	1.0	1.1	0.7	1
p-Xylene	6.5	6.2	6.4	4.1	6
m-Xylene	5.1	5.0	4.7	3.6	5.3
o-Xylene	3.9	3.1	3.1	1.7	3.4
BTEX <sup>b</sup>	27.4	24.5	22.1	14.7	20.0
C <sub>9</sub> aromatics	7.7	5.9	7.7	7.9	15.2
C <sub>6</sub> –C <sub>9</sub> aromatics <sup>c</sup>	35.1	30.5	29.8	22.6	35.2
C <sub>10</sub> aromatics	3.3	1.5	4.5	0.0	14.2

<sup>a</sup> Selectivity of C<sub>2</sub>=C<sub>4</sub>= was calculated by sum of ethene, propene, and butenes.<sup>b</sup> Selectivity of BTEX was calculated by sum of benzene, toluene, ethylbenzene, and xylenes.<sup>c</sup> Selectivity of C<sub>6</sub>–C<sub>9</sub> aromatics was calculated by sum of BTEX and C<sub>9</sub> aromatics.

conversion reached 100%, but the product selectivity changed with respect to the Gd content and the preparation method. Light olefins in the range of C<sub>2</sub> to C<sub>6</sub> showed a tendency to increase in selectivity as the Gd content increased. In particular, the selectivity toward propene and

butene using the 1GdHZ and 5GdHZ catalysts was twice as much as that of the HZ catalyst, and five and three times as much higher, respectively, using the 10GdHZ catalyst. Notably, the selectivity toward ethene slightly increased as the amount of Gd increased (up to 5 wt%), but the selectivity obtained from the 10GdHZ catalyst for this product was nearly zero. The selectivity toward light paraffins decreased slightly with increasing Gd content. The selectivity toward formation of aromatics, including benzene, toluene, ethylbenzene, and xylene (BTEX), C<sub>9</sub>, and C<sub>10</sub>, also showed the same tendency as that for the light paraffins; however, the 5GdHZ and 1GdHZ catalysts provided similar selectivity of aromatic compounds. In the case of the GdHZ-IE catalyst, the selectivity toward the formation of light paraffins was reduced by half, and the selectivities toward the C<sub>9</sub> and C<sub>10</sub> aromatics were two and four times greater, respectively, than that of the HZ catalyst.

The changes in the methanol conversion and product selectivity using the Gd-modified HZSM-5 catalysts during 70 h on stream of the MTH reaction are shown in Fig. 5. Before the performance test, only Gd<sub>2</sub>O<sub>3</sub> powder was loaded in the reactor bed and it did not show any reactivity (not shown here) in MTH reaction under the given conditions. For the catalysts prepared by the impregnation method, the methanol conversion was maintained close to 100% for a longer time as the content of Gd increased (Fig. 5-A), while the periods for maintaining a methanol conversion of 95% were 42, 54, and 64 h for 1GdHZ, 5GdHZ, and 10GdHZ, respectively. Moreover, the slope of the conversion decreased gradually and became moderate with increasing Gd content; the conversion of methanol over the HZ catalyst provided the lowest value of 76% at a reaction time of 70 h while that of the 10GdHZ catalyst maintained the highest value of 92% during the same time. Similar to the results of methanol conversion, the selectivity of aromatics was further reduced with the increasing Gd content (Fig. 5C–E). It is worth noting that the 5GdHZ catalyst (Fig. 5D) exhibited a similar result to that for the 1GdHZ catalyst (not an intermediate value between that for the 1GdHZ and 10GdHZ catalysts). The selectivities toward paraffins and aromatics steadily decreased during the 70 h MTH reaction, while those toward light olefins gradually increased at the beginning of the reaction and then decreased from the point at which dimethyl ether (DME) started to be produced in the reaction; in particular, degree of the change of the C<sub>2</sub>–C<sub>4</sub> light olefins is large. Meanwhile, the GdHZ-IE catalyst showed a different reactivity than the Gd/HZSM-5 catalysts prepared by the impregnation method. The time at which the methanol conversion started to decrease was earlier than that of the HZ catalyst, while the selectivity toward aromatic compounds (particularly C<sub>10</sub> aromatics) was higher.

### 3.3. Characterization of coke

The catalysts were collected at a reaction time of 20 h and analyzed by FT-IR spectroscopy and TPO techniques to investigate the structure, quantity, and burn-off characteristics of the coke formed on the Gd-modified ZSM-5 catalysts during the MTH reaction. As shown in Fig. 6,

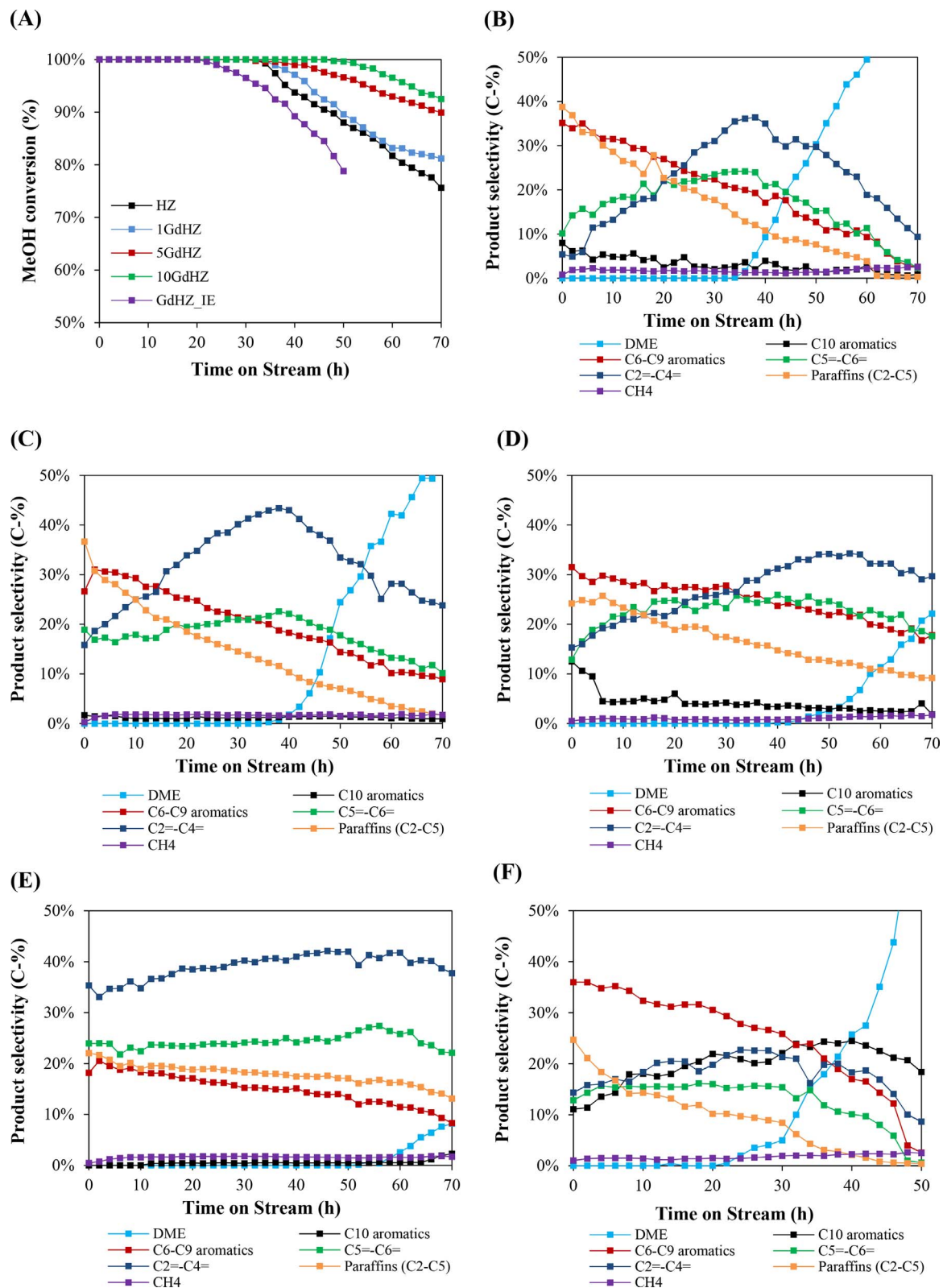


**Fig. 5.** Comparison of the catalytic activities of the Gd modified HZSM-5 catalysts in the MTH reaction: (A) MeOH conversion and product selectivity for (B) HZ, (C) 1GdHZ, (D) 5GdHZ, (E) 10GdHZ, and (F) GdHZ<sub>IE</sub>.

the IR spectra of all the catalysts exhibited typical characteristics of paraffinic and aromatic structured coke deposits in the region 2700–3100 cm<sup>-1</sup> (Fig. 6A) and 1300–1700 cm<sup>-1</sup> (Fig. 6B). For instance, the stretching vibrations of the –CH<sub>3</sub> groups appear at ~2970 cm<sup>-1</sup> and 2840 cm<sup>-1</sup> and those of the –CH(CH<sub>2</sub>) groups appear

at ~2950–2920 cm<sup>-1</sup> and 2870 cm<sup>-1</sup>. The IR peaks appearing at 1620, 1588, 1540, 1440, and 1365 cm<sup>-1</sup> are associated with the C=C stretching vibrations of unsaturated hydrocarbons, C–H bending vibration of complex aromatics (so-called polycondensed aromatic coke species), C–C stretching vibration of naphthalene, CH twisting

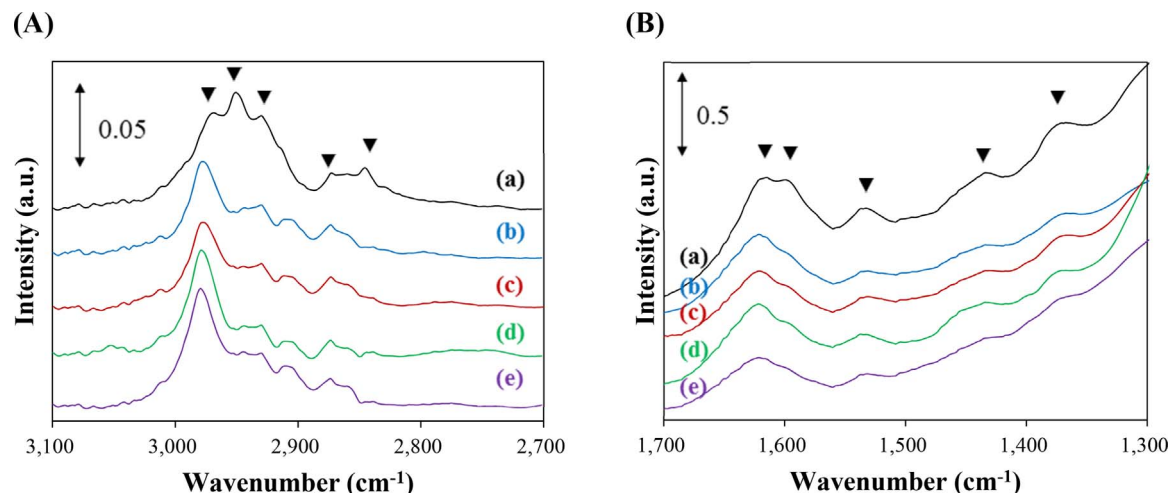


Fig. 6. FT-IR spectra in (A) region  $2700 - 3100\text{ cm}^{-1}$  and (B) region  $1300 - 1700\text{ cm}^{-1}$  of the spent (a) HZ, (b) 1GdHZ, (c) 5GdHZ, (d) 10GdHZ, and (e) GdHZ\_IE collected after 20 h of the MTH reaction.

vibrations of complex aromatics, and CH wagging vibrations of complex aromatics, respectively [27,33–36]. For the HZ catalyst, the conversions to the longer paraffinic carbon chain and the polycondensed aromatic species are both noticeably more than that obtained using the Gd/HZSM-5 catalysts, with which the formation of such molecules is inhibited irrespective of the Gd content. In the case of the GdHZ\_IE catalyst, the intensity of the IR peak corresponding to the complex aromatic structures is reduced, while that of the IR peak corresponding to the  $-\text{CH}_3$  groups is increased when compared with those for the Gd-modified HZSM-5 catalysts prepared by the impregnation method.

The amount of carbon deposited on the collected catalysts after 20 h of the MTH reaction and its burn-off characteristics were also investigated using TPO analysis. As shown in Fig. 7, the intensity of the major TPO peak was highest for the HZ catalyst, and the intensity decreased as the content of Gd increased. The TPO peak areas (table in Fig. 7) were reduced to 51, 49, 46, and 44% compared to the peak area of the HZ catalyst for the 1GdHZ, 5GdHZ, 10GdHZ, and GdHZ\_IE catalysts, respectively. The increase in the Gd content reduced the temperature at which the TPO peak reaches its maximum value. Furthermore, carbon was observed to have burned off in a low temperature zone between 200 and 500 °C on the Gd/HZSM-5 catalysts (Fig. S4); a significant amount of carbon was burned off at 250 °C and 400 °C for

the 10GdHZ catalyst.

#### 3.4. Role of Gd in reactivity and stability of the Gd promoted ZSM-5 catalyst

The effect of Gd metal, which is used to enhance the lifetime of the HZSM-5 catalyst by decreasing coke deposition during the MTH reaction, has been previously demonstrated. In this study, the effect of the Gd loading amount and the preparation method on the reactivity, physical and chemical natures, deactivation, and coke formation of the Gd-modified ZSM-5 catalyst in the MTH reaction were investigated.

The Gd metal present on the surface of the HZSM-5 catalyst in the form of a film, more accurately  $\text{Gd}_2\text{O}_3$ , was first identified in previous studies: Gd metal with an invariant valence (+3) forms a stable six-coordinate complex with oxygen atoms, yet three of the oxygen atoms are engaged in the zeolite framework [29]. It was also found that increasing the content of Gd metal on HZSM-5 does not create a thicker film, but rather more crystals are uniformly covered by nano-sized  $\text{Gd}_2\text{O}_3$  particles or a thin film of a uniform thickness on the surface of the ZSM-5 crystal. The  $\text{N}_2$  adsorption-desorption results (Table 1) and XRD analysis (Fig. 1) support this finding. As the Gd content increases, the area of the thin film covering the HZSM-5 crystal also increases, linearly reducing the surface area and pore volume of the Gd/HZSM-5 catalysts. In addition, the entrance of the mesopores also becomes smaller and  $\text{N}_2$  desorption increases at lower relative pressures (Fig. S5). However, the GdHZ\_IE catalyst shows almost no change in the XRD peak intensity (Fig. 1), surface area, and pore volume (Table 1), even though the Gd content is nearly 4 wt%. The  $\text{Gd}^{3+}$  cations are only ion-exchanged with the protons of HZSM-5 and are not physically adsorbed on the crystal surface to form a thin film. In fact, the mesopore volume likely increases because of the removal of impurities in the mesopore spaces during the washing steps when preparing the catalyst by the ion exchange method (Table 1).

An explanation for the observation of change in the product selectivity over time for the HZ and Gd/HZSM-5 catalysts (Fig. 5) is that when the methanol conversion starts decreasing, DME is formed and the production of olefins reduces. In particular, there was no noticeable decrease in olefin production for the 10GdHZ catalyst during 70 h of the MTH reaction. In contrast, the decreased selectivity toward paraffins and aromatics, including BTEX, shows a gradual decrease from the beginning of the reaction irrespective of the decrease in methanol conversion.

The change in selectivity over time for  $\text{C}_2-\text{C}_4$  olefins is more interesting (Fig. 8). No ethene is produced when the 10GdHZ catalyst is used, which suggests that the pathway of methanol to aromatics

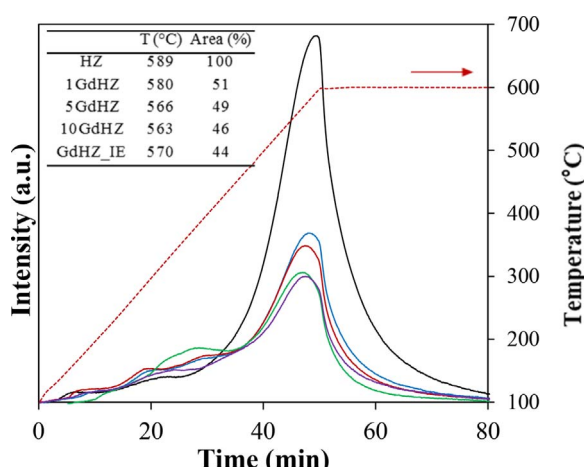


Fig. 7. TPO curves of the spent (black line) HZ, (blue line) 1GdHZ, (red line) 5GdHZ, (green line) 10GdHZ, and (purple line) GdHZ\_IE collected after 20 h of MTH reaction. The table in the figure summarizes the temperature at which the maximum intensity appears and the relative area of the peak with respect to HZ. (For interpretation of the references to colour in this figure legend, the reader is referred to the web version of this article.)

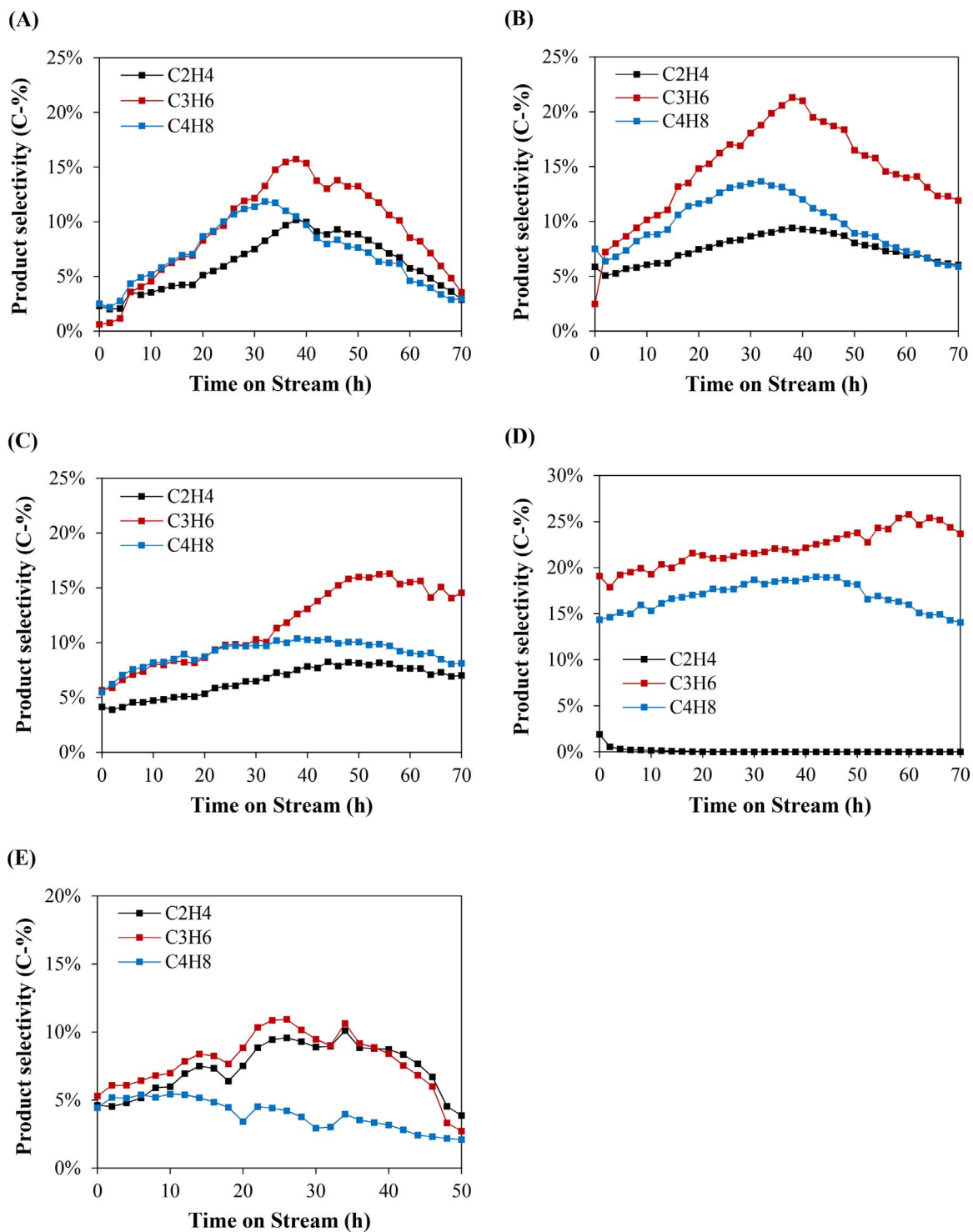


Fig. 8. Selectivity of  $\text{C}_2\text{H}_4$ ,  $\text{C}_3\text{H}_6$ , and  $\text{C}_4\text{H}_8$  over the (A) HZ, (B) 1GdHZ, (C) 5GdHZ, (D) 10GdHZ, and (E) GdHZ-IE catalysts during the MTH reaction.

conversion is altered by the deposition of Gd. It should be noted that the acidity of the Gd modified catalysts changes with the Gd content. The LAS decrease significantly in number for the Gd/HZSM-5 catalysts prepared by the impregnation method (Table 2). As shown in Fig. 9, the number of LAS of the HZ and Gd/HZSM-5 catalysts and their selectivity toward paraffins and aromatic compounds exhibit a linear correlation. A possible explanation of these result is the different hydrogen transfer rates between methanol molecules and intermediate products during the MTH reaction. Gasified methanol molecules are first adsorbed onto Brønsted acid sites (BAS) where they undergo a dehydration reaction

regardless of whether  $\text{CH}_3$  or  $\text{CH}_3\text{O}$  intermediates are formed [7,37–41]. More importantly, the hydrogen exchange reaction between methanol and the first-formed olefin becomes very active on the acidic sites of the HZSM-5 catalyst [42–44]. Muller and co-workers have recently reported that the first-formed olefins, particularly propene, act as hydrogen acceptors and methanol acts as a hydrogen donor, resulting in the formation of formaldehyde in a short time on the Lewis acid sites (LAS) [43]. Subsequently, formaldehyde might then be transformed to  $\text{H}_2\text{O}$  and a hydrogen-poor diene intermediate via dehydration, along with other olefins on the BAS. This continuous reaction forms a

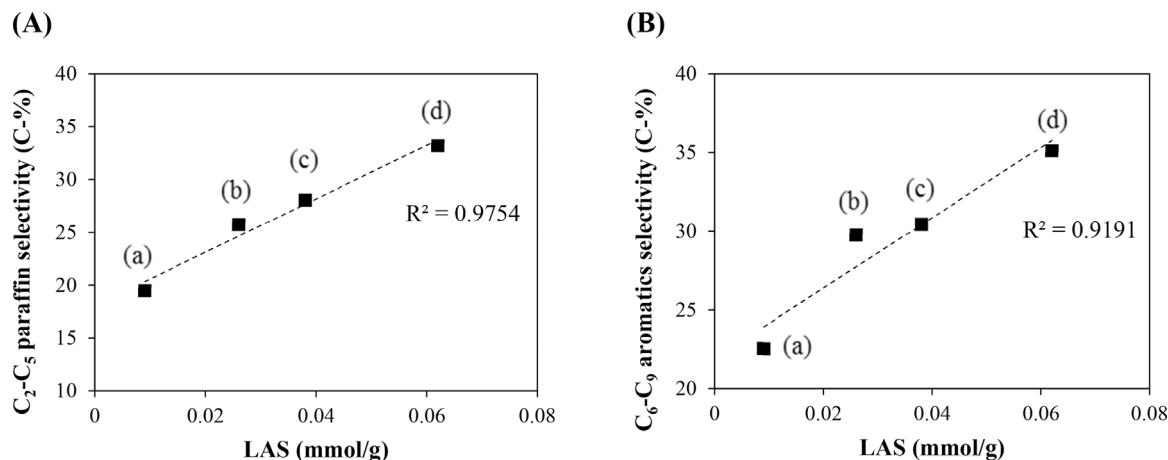


Fig. 9. (A)  $C_2-C_5$  paraffin selectivity and (B)  $C_6-C_9$  aromatics selectivity as a function of Lewis acid sites: (a) 10GdHZ, (b) 5GdHZ, (c) 1GdHZ, and (d) HZ.

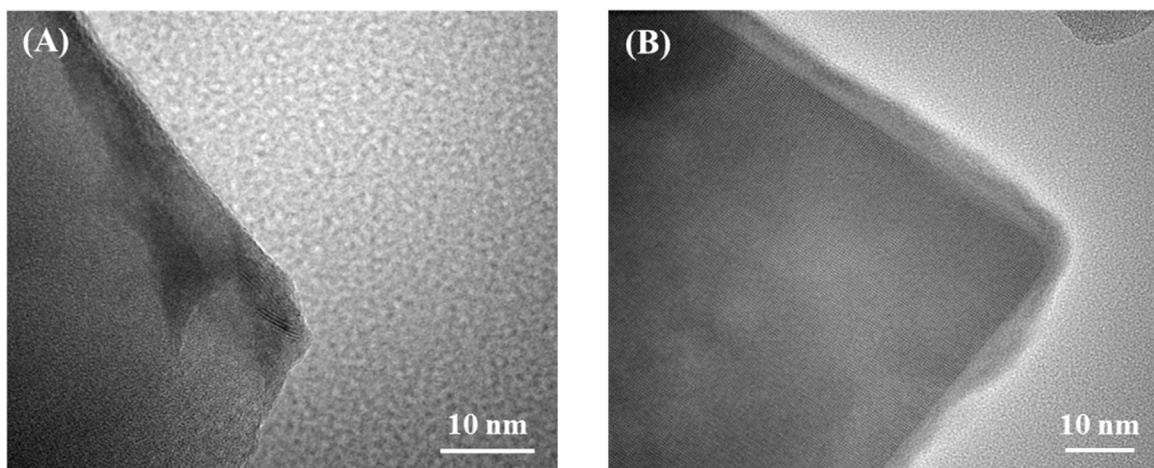


Fig. 10. STEM images of the (A) spent 10GdHZ catalyst and (B) spent HZ catalyst after 70 h of a MTH reaction.

hydrogen poor, long carbon chain until finally light olefins, paraffins, and aromatics are produced via a series of reactions [7,42,45]. Additionally, the alkane produced during the reaction is transformed into  $C_2H_4$  and other olefin molecules by  $\beta$ -scission [7,46,47]. In this work, as the amount of LAS and BAS decreases, the amount of formaldehyde and diene intermediates generated during the reaction also decreases, thereby reducing the production of paraffins and aromatics.

In contrast, after the methanol dehydration reaction, the carbon chain growth proceeds more on the BAS, resulting in an increase in the production of olefins as the Gd content increases. Transient formation of formaldehyde would likely not take place if LAS were not present. This implies that the formation of a saturated alkane is not also expected to occur (Fig. 9-A) and the resulting  $\beta$ -scission would also not proceed, thus eliminating the opportunity for  $C_2H_4$  formation (Fig. 8-D). The light olefins, aromatics, and paraffins are presumably produced by chain growth, olefin oligomerization, aromatization, and hydrogen transfer between the aromatic intermediates and light olefins, and referring to the olefin-induced hydrogen transfer, on the BAS without the involvement of LAS when the 10GdHZ catalyst was used. The decreased methanol conversion and the onset of DME production (Fig. 5) can be deduced from the complete dehydration of methanol, which is limited by the carbonaceous species adsorbed on the BAS. As the reaction proceeds, the blocking of the BAS by carbonaceous deposits (also known as coking) becomes severe and thus, all reactions catalyzed by the BAS are expected to be limited.

On the other hand, the existing BAS are transformed into the LAS by the ion-exchanged Gd in the GdHZ<sub>IE</sub> catalyst, and the LAS become

stronger than the corresponding sites in the HZ catalyst (Table 2). As a result, an amazingly low selectivity toward olefins and a high selectivity toward aromatic compounds (particularly the  $C_9$  and  $C_{10}$  aromatics) is observed (Table 3, Figs. 5-F, and S6). This indicates that a high degree of benzene ring methylation reaction are formed at the acidic sites. This trend increases with reaction time and thereby increases the catalyst deactivation. As the catalyst life time is shorter for the Gd-modified ZSM-5 catalysts in comparison with the HZ catalyst, this deactivation cannot be attributed to on-surface-coking but instead to the accumulation of aromatics with 4- or 5-methyl groups in the pores. Furthermore, the Gd-ions in the pores may cause constraints on diffusion, leading to longer residence times of the product species in the pores. This phenomenon favors secondary reactions, specifically benzene ring methylation by reaction with methanol [10]. An increase in the production of aromatic compounds over the metal ion-exchanged ZSM-5 catalyst has been previously reported [48,49]; the GdHZ<sub>IE</sub> catalyst is accordingly also expected to follow that trend. Furthermore, the observed ethene and propene selectivities (Table 3 and Fig. 8-E) also support the hypothesis that an aromatic-based cycle pathway is predominant during the MTH reaction [46,50].

The analysis of the spent HZ and Gd/HZSM-5 catalysts shows the inhibiting effects of Gd on coke formation. Fig. 10 shows that the deposition of carbon on the thin film covering the HZSM-5 crystal is not observed after 70 h of MTH reaction; in contrast, formation of amorphous carbon on the crystals of the HZ is observed. In addition, based on the FT-IR spectra, complex-structured aromatic or graphite-like deposits (possible products of further methylation and dehydrogenation of

mono- or dicyclic aromatics [10,51]) appear from the spent HZ (Fig. 6B). The TPO curves of the catalysts also indicate varying amounts of coke deposited on the catalysts during the reaction. Notably, regardless of the Gd content and the preparation method, an addition of Gd on the HZSM-5 catalyst hinders carbon deposition and the formation of the complex-structured coke during a MTH reaction. The presence of  $\text{Gd}_2\text{O}_3$  on the surface is expected to hinder the adsorption of carbocation intermediates as well as further growth of the aromatic-structured coke by increasing basicity and spatial constraints of the bare ZSM-5 [52]. In case of the GdHZ-IE catalyst, the Lewis acid sites created in addition to the existing ones by substituting the framework protons with  $\text{Gd}^{3+}$  cations led to the hydrogenation ability of the bare ZSM-5. The oxidation of coke on the periphery of the thin film covering the HZSM-5 crystal could be catalyzed by oxygen mobility with  $\text{Gd}_2\text{O}_3$  or an ion-exchanged Gd cation [53]. Thus, regenerability is yet another advantage of Gd modification of the HZSM-5 catalyst.

In conclusion, a coke tolerant characteristic of the ZSM-5 catalyst can be gained by the Gd loading regardless of its content and preparation method. However, product selectivity of the catalysts is also modified by those factors as well. Although the catalytic lifetime can be prolonged by increasing the Gd content when it prepared by an impregnation method, it is necessary to consider that the pathway for aromatics is suppressed while that for alkenes is enhanced. Therefore, one can choose an optimum range of the Gd content and a preparation method to attain specific conditions or goals.

#### 4. Conclusion

In this paper, we comprehensively studied the influence of different loading amounts of Gd and the preparation method on the physical properties, acid-base characteristics, reactivity, and coke formation of the Gd/HZSM-5 catalysts in the MTH reaction. As the Gd content was increased, the area of the thin film covering the HZSM-5 crystal also increased, which linearly reduced the surface area and pore volume of the Gd/HZSM-5 catalysts. However, an increase in the Gd content did not lead to a thicker film. In contrast, in the case of the catalyst prepared by the ion exchange method, no changes in crystallinity, surface area, and pore volume were found. The number of strong acid sites typically decreased with respect to the amount of Gd. Furthermore, it was revealed that the Gd metal ion exchange with the BAS produced strong LAS and consequently the L/B ratio became greater than that of the basic ZSM-5 catalyst. Contrary to changes in acidic properties, the basicity of the Gd/HZSM-5 catalysts increased in proportion to the increased Gd content. Changes in the acid-base properties of the HZSM-5 catalyst by an addition of Gd confirmed the significant effect on the catalytic activity and the reaction mechanism in the MTH reaction. The selectivity of light olefins increased with increasing Gd content, and the selectivities toward light paraffins and aromatic compounds decreased. This is likely a result of the change of the hydrogen transfer characteristics of the catalyst because of the lesser number of LAS. The Gd/HZSM-5 catalyst prepared by the ion exchange method showed a high aromatic selectivity because of the large number of strong LAS. The addition of Gd inhibited the deposition of carbon species and formation of aromatic molecules with complex structures, thereby decreasing the amount of carbon deposition by more than 50%. As a result, the effect of improving the catalyst deactivation with respect to the Gd content on the HZSM-5 catalysts in the MTH reaction was clearly observed. In summary, the physicochemical properties and reactivities of the Gd-modified ZSM-5 catalysts greatly depend on the Gd content and the preparation method. Based on these findings, an optimum use of Gd, including a preparation method for zeolite-based catalysts, should be determined for not only a MTH reaction, but also for other hydrocarbon conversion reactions. In addition, the role and use of Gd metal in the bimetallic system has not yet been elucidated, and thus, further research should continue.

#### Acknowledgment

This work was further financially supported by the core KRICT project (SI1701-06) from Korea Research Institute of Chemical Technology

#### Appendix A. Supplementary data

Supplementary data associated with this article can be found, in the online version, at <http://dx.doi.org/10.1016/j.apcatb.2017.08.056>.

#### References

- [1] S. Kulprathipanja, *Zeolites in Industrial Separation and Catalysis*, Wiley-VCH, Weinheim, 2010.
- [2] J. García-Martínez, K. Li, *Mesoporous Zeolites Preparation, Characterization and Applications*, Wiley-VCH, Hoboken, 2015.
- [3] G.K.H.W.J. Ertl, *Handbook of Heterogeneous Catalysis*, Wiley-VCH, Weinheim, 1997.
- [4] J.F. Haw, W. Song, D.M. Marcus, J.B. Nicholas, The mechanism of methanol to hydrocarbon catalysis, *Acc. Chem. Res.* 36 (2003) 317–326.
- [5] O. Unni, S. Stian, B. Morten, B. Pablo, J. Finn, B. Silvia, Conversion of methanol to hydrocarbons: how zeolite cavity and pore size controls product selectivity, *Angew. Chem. Int. Ed.* 51 (2012) 5810–5831.
- [6] S. Teketel, U. Olsbye, K.-P. Lillerud, P. Beato, S. Svelle, Selectivity control through fundamental mechanistic insight in the conversion of methanol to hydrocarbons over zeolites, *Microporous Mesoporous Mater.* 136 (2010) 33–41.
- [7] S. Ilias, A. Bhan, Mechanism of the catalytic conversion of methanol to hydrocarbons, *ACS Catal.* 3 (2013) 18–31.
- [8] M. Stocker, Methanol-to-hydrocarbons: catalytic materials and their behavior, *Microporous Mesoporous Mater.* 29 (1999) 3–48.
- [9] Y. Ono, Transformation of lower alkanes into aromatic hydrocarbons over ZSM-5 zeolites, *Catal. Rev.* 34 (1992) 179–226.
- [10] H. Schulz, M. Wei, Pools and constraints in methanol conversion to olefins and fuels on zeolite HZSM5, *Top. Catal.* 57 (2014) 683–692.
- [11] H. Schulz, Coking of zeolites during methanol conversion: basic reactions of the MTO-, MTP- and MTG processes, *Catal. Today* 154 (2010) 183–194.
- [12] M. Guisnet, P. Magnoux, Organic chemistry of coke formation, *Appl. Catal. A* 212 (2001) 83–96.
- [13] M. Guisnet, L. Costa, F.R. Ribeiro, Prevention of zeolite deactivation by coking, *J. Mol. Catal. A* 305 (2009) 69–83.
- [14] D. Chen, K. Moljord, A. Holmen, A methanol to olefins review: diffusion, coke formation and deactivation SAPO type catalysts, *Microporous Mesoporous Mater.* 164 (2012) 239–250.
- [15] D.M. Bibby, Coke formation in high-silica zeolites, *Appl. Catal. A* 93 (1992) 1–34.
- [16] P.D. Hopkins, J.T. Miller, B.L. Meyers, G.J. Ray, R.T. Roginski, M.A. Kuehne, H.H. Kung, Acidity and cracking activity changes during coke deactivation of ultrastable Y zeolite, *Appl. Catal. A* 136 (1996) 29–48.
- [17] J. Kim, M. Choi, R. Ryoo, Effect of mesoporosity against the deactivation of MFI zeolite catalyst during the methanol-to-hydrocarbon conversion process, *J. Catal.* 269 (2010) 219–228.
- [18] G.Q. Zhang, T. Bai, T.F. Chen, W.T. Fan, X. Zhang, Conversion of methanol to light aromatics on Zn-modified nano-HZSM-5 zeolite catalysts, *Ind. Eng. Chem. Res.* 53 (2014) 14932–14940.
- [19] Z. Wei, T. Xia, M. Liu, Q. Cao, Y. Xu, K. Zhu, X. Zhu, Alkaline modification of ZSM-5 catalysts for methanol aromatization: the effect of the alkaline concentration, *Front. Chem. Sci. Eng.* 9 (2015) 450–460.
- [20] X. Wang, J. Zhang, T. Zhang, H. Xiao, F. Song, Y. Han, Y. Tan, Mesoporous ZnZSM-5 zeolites synthesized by one-step desilication and reassembly: a durable catalyst for methanol aromatization, *RSC Adv.* 6 (2016) 23428–23437.
- [21] J. Huang, Y.J. Jiang, V.R.R. Marthala, A. Bressel, J. Frey, M. Hunger, Effect of pore size and acidity on the coke formation during ethylbenzene conversion on zeolite catalysts, *J. Catal.* 263 (2009) 277–283.
- [22] M. Ibáñez, M. Gánero, J. Ruiz-Martínez, B.M. Weckhuysen, A.T. Aguayo, J. Bilbao, P. Castaño, Simultaneous coking and dealumination of zeolite H-ZSM-5 during the transformation of chloromethane into olefins, *Catal. Sci. Technol.* 6 (2016) 296–306.
- [23] M.O. Adebajo, M.A. Long, The contribution of the methanol-to-aromatics reaction to benzene methylation over ZSM-5 catalysts, *Catal. Commun.* 4 (2003) 71–76.
- [24] C. Sun, Y. Yang, J. Du, F. Qin, Z. Liu, W. Shen, H. Xu, Y. Tang, Dehydrogenation inhibition on nano-Au/ZSM-5 catalyst: a novel route for anti-coking in methanol to propylene reaction, *Chem. Commun.* 48 (2012) 5787–5789.
- [25] M. Inaba, K. Murata, M. Saito, I. Takahara, Ethanol conversion to aromatic hydrocarbons over several zeolite catalysts, *React. Kinet. Catal. Lett.* 88 (2006) 135–142.
- [26] H. Ren, M.P. Humbert, C.A. Menning, J.G. Chen, Y. Shu, U.G. Singh, W.-C. Cheng, Inhibition of coking and CO poisoning of Pt catalysts by the formation of Au/Pt bimetallic surfaces, *Appl. Catal. A* 375 (2004) 303–309.
- [27] S. Kim, E. Sasmaz, J. Lauterbach, Effect of Pt and Gd on coke formation and regeneration during JP-8cracking over ZSM-5 catalysts, *Appl. Catal. B* 168 (2015) 212–219.
- [28] R. Bal, B. Sarkar, R. Kumar, S. Acharyya, S. Ghosh, Coke Resistant Solid Catalyst

Process for the Preparation Thereof and a Process for Vapour Phase Dry Reforming of Methane, Council of Scientific & Industrial Research, US, 2014.

[29] S. Kim, Y.T. Kim, A. Hwang, K.-W. Jun, G. Kwak, Coke-tolerant gadolinium-promoted HZSM-5 catalyst for methanol conversion into hydrocarbons, *ChemCatChem* 9 (2017) 1–6.

[30] M. Guisnet, P. Ayrault, J. Datka, Acid properties of dealuminated mordenites studied by IR spectroscopy. 2. Concentration, acid strength and heterogeneity of OH groups, *Pol. J. Chem.* 71 (1997) 1455–1461.

[31] N. Rahimi, R. Karimzadeh, Catalytic cracking of hydrocarbons over modified ZSM-5 zeolites to produce light olefins: a review, *Appl. Catal. A* 398 (2011) 1–17.

[32] R.J. Gorte, Design parameters for temperature programmed desorption from porous catalysts, *J. Catal.* 75 (1982) 164–174.

[33] H.G. Karge, W. Niessen, H. Bludau, In-situ FTIR measurements of diffusion in coking zeolite catalysts, *Appl. Catal. A* 146 (1996) 339–349.

[34] P. Castaño, G. Elordi, M. Olazar, A.T. Aguayo, B. Pawelec, J. Bilbao, Insights into the coke deposited on HZSM-5, H $\beta$  and HY zeolites during the cracking of polyethylene, *Appl. Catal. B* 104 (2011) 91–100.

[35] N. Martí, M. Viniegra, E. Lima, G. Espinosa, Coke characterization on Pt Al2O3 βzeolite reforming catalysts, *Ind. Eng. Chem. Res.* 43 (2004) 1206–1210.

[36] S.V. Donk, E. Bus, A. Broersma, J.H. Bitter, K.P.D. Jong, Probing the accessible sites for n-butene skeletal isomerization over aged and selective H-ferrierite with d3-Acetonitrile, *J. Catal.* 212 (2002) 86–93.

[37] P.G. Moses, J.K. Nørskov, Methanol to dimethyl ether over ZSM-22: a periodic density functional theory study, *ACS Catal.* 3 (2013) 735–745.

[38] D. Lesthaeghe, V.V. Speybroeck, G.B. Marin, M. Waroquier, What role do oxonium ions and oxonium ylides play in the ZSM-5 catalysed methanol-to-olefin process? *Chem. Phys. Lett.* 417 (2006) 309–315.

[39] D. Lesthaeghe, V.V. Speybroeck, G.B. Marin, M. Waroquier, The rise and fall of direct mechanisms in methanol-to-Olefin catalysis: an overview of theoretical contributions, *Ind. Eng. Chem. Res.* 46 (2007) 8832–8838.

[40] I.M. Dahl, S. Kolboe, On the reaction mechanism for propene formation in the MTO reaction over SAPO-34, *J. Catal.* 149 (1994) 458–464.

[41] D.M. Marcus, K.A. McLachlan, M.A. Wildman, J.O. Ehrmann, P.W. Kletnieks, J.F. Haw, Experimental evidence from H/D exchange studies for the failure of direct C–C coupling mechanisms in the methanol-to-olefin process catalyzed by HSAPO-34, *Angew. Chem.* 118 (2006) 3205–3208.

[42] X. Sun, S. Mueller, Y. Liu, H. Shi, G.L. Haller, M. Sanchez-Sanchez, A.C.V. Veen, J.A. Lercher, On reaction pathways in the conversion of methanol to hydrocarbons on HZSM-5, *J. Catal.* 317 (2014) 185–197.

[43] S. Müller, Y. Liu, F.M. Kirchberger, M. Tonigold, M. Sanchez-Sanchez, J.A. Lercher, Hydrogen transfer pathways during zeolite catalyzed methanol conversion to hydrocarbons, *J. Am. Chem. Soc.* 138 (2016) 15994–16003.

[44] V.B. Kazansky, M.V. Frash, R.A.V. Santen, A quantum-chemical study of hydride transfer in catalytic transformations of paraffins on zeolites. Pathways through adsorbed nonclassical carbonium ions, *Catal. Lett.* 48 (1997) 61–67.

[45] M. Björgen, U. Olsbye, D. Petersen, S. Kolboe, The methanol-to-hydrocarbons reaction: insight into the reaction mechanism from [12C] benzene and [13C] methanol coreactions over zeolite H-beta, *J. Catal.* 221 (2004) 1–10.

[46] S. Wang, Y. Chen, Z. Wei, Z. Qin, H. Ma, M. Dong, J. Li, W. Fan, J. Wang, Polymethylbenzene or alkene cycle? Theoretical study on their contribution to the process of methanol to olefins over H-ZSM-5 zeolite, *J. Phys. Chem. C* 119 (2015) 28482–28498.

[47] I.M. Dahl, S. Kolboe, On the reaction mechanism for hydrocarbon formation from methanol over SAPO-34: 2. Isotopic labeling studies of the co-reaction of propene and methanol, *J. Catal.* 161 (1996) 304–309.

[48] S.-W. Choi, W.-G. Kim, J.-S. So, J.S. Moore, Y. Liu, R.S. Dixit, J.G. Pendergast, C. Sievers, D.S. Sholl, S. Nair, C.W. Jones, Propane dehydrogenation catalyzed by gallosilicate MFI zeolites with perturbed acidity, *J. Catal.* 345 (2017) 113–123.

[49] M. Conte, J.A. Lopez-Sánchez, Q. He, D.J. Morgan, Y. Ryabenkova, J.K. Bartley, A.F. Carley, S.H. Taylor, C.J. Kiely, K. Khalid, G.J. Hutchings, Modified zeolite ZSM-5 for the methanol to aromatics reaction, *Catal. Sci. Technol.* 2 (2012) 105–112.

[50] T. Liang, J. Chen, Z. Qin, J. Li, P. Wang, S. Wang, G. Wang, M. Dong, W. Fan, J. Wang, Conversion of methanol to olefins over H-ZSM-5 zeolite: reaction pathway is related to the framework aluminum siting, *ACS Catal.* 6 (2016) 7311–7325.

[51] D. Eisenbach, E. Gallei, Infrared spectroscopic investigations relating to coke formation on zeolites, *J. Catal.* 56 (1979) 377–389.

[52] X. Wang, Z. Zhao, C. Xu, D. Aijun, L. Zhang, J. Guiyuan, Effects of light rare earth on acidity and catalytic performance of HZSM-5 zeolite for catalytic cracking of butane to light olefins, *J. Rare Earth* 25 (2007) 321–328.

[53] A. Barrera, M. Viniegra, S. Fuentes, G. Diaz, The role of lanthana loading on the catalytic properties of Pd/Al2O3-La2O3 in the NO reduction with H-2, *Appl. Catal. B* 56 (2005) 279–288.